nature water

Article

https://doi.org/10.1038/s44221-024-00193-x

Disentangling contributions to past and future trends in US surface soil moisture

Received: 20 April 2023

Accepted: 3 January 2024

Published online: 05 February 2024

Check for updates

Lucas R. Vargas Zeppetello [1] ✉, Aleyda M. Trevino [1,2] & Peter Huybers [1]

Climate model simulations and various aridity indices generally indicate that summertime surface soil moisture will decrease in the continental USA as a consequence of anthropogenic climate change. However, soil moisture observations from ground probes and satellites from 2011 to 2020 indicate positive summertime trends across 57% of the continental USA. To evaluate the mechanisms driving these trends, we have developed a two-layer land surface model that predicts surface temperature and soil moisture on the basis of observed variations in precipitation, solar radiation, vapour pressure and snowmelt. Of these four model forcings, we found that internal precipitation variability explains the largest fraction of the observed soil moisture trends from 2011 to 2020. Surface air warming and the response of plants to increasing atmospheric CO_2 also influence the soil moisture trends, but these effects are small at decadal timescales and partly compensate for one another. Looking forwards, our results indicate that internal precipitation variability will dictate decadal soil moisture trends and that centennial soil moisture trends will primarily depend on changes in precipitation that are currently highly uncertain.

Soil moisture is a key state variable that characterizes hydrological conditions across the global land surface. Heat waves, flooding, wildfires and crop yields are all tied to variations in soil moisture[1–4]. Accurate predictions of how climate change will affect humanity require a physical understanding of soil moisture variability on timescales ranging from days[5] to seasons[6] to centuries[7,8]. Observing soil moisture from ground- and space-based platforms has been a major challenge as soils are highly heterogeneous in both the horizontal and vertical dimensions[9–12]. Satellite observations may penetrate deeper than a few centimetres into the soil column[13], but the extent to which they capture dynamics deeper than, at best, the first few tens of centimetres is generally not known. In part due to these difficulties, very few studies have examined long-term variations in surface soil moisture, and these have indicated both increasing[14] and decreasing[15] surface soil moisture trends in satellite-derived observations taken between the late 1970s and mid-2000s.

In the absence of long-running and rigorously validated global soil moisture observations, many studies of terrestrial climate rely on large-scale land surface models. These models are either components of general circulation models or stand-alone models that are forced by meteorological inputs and are often referred to as 'offline simulations'. Large biases in global climate model representations of soil moisture relative to available observations, however, make them difficult to use as tools for understanding observed surface soil moisture variability[16]. Possibly due to these underlying biases, global climate models have difficulty reproducing historical trends from in situ soil moisture observations[17]. Another challenge that prevents a detailed understanding of soil moisture variability is that different model representations of soil moisture cannot be directly compared with one another. Soil moisture in some models is represented as an 'index' rather than a physical state variable[18], an issue that has persisted in the latest generation of models that participated in the Coupled Model Intercomparrison Project Phase 6 (CMIP6) experiments[19]. For example, the evapotranspiration associated with a dry-season surface soil moisture of 0.25 m^3 water per m^3 soil (0.25 m^3 m^{-3}) in one model might correspond to the evapotranspiration produced by a soil moisture of 0.05 m^3 m^{-3} in another model. Although scaling procedures can be used to indirectly compare soil moisture output across models, the different parameterizations

[1]Department of Earth and Planetary Science, Harvard University, Cambridge, MA, USA. [2]Department of Earth and Climate Sciences, San Francisco State University, San Francisco, CA, USA. ✉e-mail: vargas_zeppetello@berkeley.edu

that depend on model-specific representations of soil moisture make model intercomparison challenging[20].

Given the difficulty of physically interpreting soil moisture output from climate models, a complementary approach to understanding hydroclimate variability is based on metrics that can be derived from observations and used as proxies for surface soil moisture. The Aridity Index, Potential Evapotranspiration and the Palmer Drought Severity Index have all been used to study global aridity[21]. Previous studies have used these metrics to argue that global drylands will intensify and expand in response to global climate change[22–25]. Although these results have been critiqued[26,27], the fact that the climate models participating in CMIP5 and CMIP6 predict reductions in surface soil moisture as a response to global warming makes understanding these long-term soil moisture trends a research priority[7,8,28].

In this Article, we show that there is no observational evidence for large-scale soil drying in response to warming in the continental USA over the past decade. An analysis of two independent observational datasets shows a consistent spatial pattern of summertime (June, July and August (JJA)) soil moisture trends over the past decade. Of particular interest is the finding that surface soil moisture has increased across 57% of the continental USA during this period, in apparent contrast to predictions of large-scale surface drying driven by increasing temperatures. The biases present in large-scale land surface models[16] indicate that idealized models have a role to play in understanding the observed variations in surface soil moisture. The first simple model of the seasonal cycle of soil moisture that used satellite observations from the Soil Moisture Active Passive satellite mission as a validation dataset was only recently published[6]. While important, this seasonal cycle model does not address interannual variability or long-term trends in surface soil moisture. In this context, we developed a simple energy and moisture balance model (EMBM) that uses observations of precipitation, solar radiation, snowmelt and vapour pressure to predict historical variability in temperature and soil moisture. We found that historical variability in precipitation is largely responsible for the soil moisture trends from 2011 to 2020. We then investigated how soil moisture may respond to anthropogenic changes in (1) surface temperature, (2) stomatal conductance and (3) precipitation in the future. In particular, we examined how likely it is that trends in surface soil moisture will be detected over the next few decades, given the uncertainty in these three possible anthropogenic changes and the presence of internal precipitation variability.

Historical trends in observations and the EMBM

Despite their small spatial footprint[9], the ground-based soil moisture measurements aggregated by the International Soil Moisture Network (ISMN) are known to be highly accurate and explain a large fraction of the daily variance in satellite observations at co-located points despite the much larger spatial footprint of the satellite observations[29]. We compared JJA soil moisture trends calculated from 102 stations in the ISMN that have adequate data at depths of 4–6 cm with satellite observations of JJA surface soil moisture compiled by the European Space Agency Climate Change Initiative (hereafter referred to as the CCI observations[30]). We were able to maximize the number of ISMN stations that passed our quality control procedure by using data from the period 2011–2020. Details of this procedure and our trend calculations are provided in Observational analysis in Methods.

The trends in the ISMN and the CCI observations are of the same order of magnitude and are significantly correlated ($P < 0.01$) across points where both measurements are available, although there is greater year-to-year variability in the JJA averages from the ISMN data than from the CCI observations that leads to some outliers (Fig. 1a,b and Supplementary Fig. 1). In both the CCI and ISMN datasets, we found increasing soil moisture across large swathes of the continental USA, particularly east of the Great Plains, where global climate models show long-term surface soil moisture reductions in response to global warming[8,28].

To understand the origin of the observed soil moisture trends, we developed a two-layer model of coupled temperature and soil moisture variability. This model builds on previous efforts to understand coupling between summertime temperature and soil moisture distributions using a one-layer model[4]. The model comprises a 10-cm-thick near-surface layer with temperature T and volumetric soil water content m_s and a 90-cm-thick deeper layer with volumetric soil water content m_d. Our results are not sensitive to the number of specified layers in our model as long as there is at least one near-surface layer overlying the deeper layer (see Sensitivity analyses in Methods and Supplementary Fig. 2). Based on the fundamental coupling between the surface energy and moisture budget equations, we refer to this as the EMBM model throughout this paper. The EMBM requires four input time series: precipitation, vapour pressure, net solar radiation and snowmelt. The precipitation and vapour pressure time series were taken from the Hadley Centre Climate Research Unit gridded time series (version 4.07)[31], net solar radiation data were from the Clouds and the Earth's Radiant Energy System (CERES) satellite[32], and monthly snowmelt was calculated from Fifth generation European Centre for Medium-Range Weather Forecasts reanalysis product (ERA5) reanalysis data[33]. We did not include human-induced fluxes of water driven by irrigation, although these are known to be substantial in some regions[34].

To conduct a 'historical' simulation, we used 40 years of data (1981–2020) for the precipitation, vapour pressure and snowmelt time series. CERES data were available from 2000 to 2020. For earlier years, we used the climatological seasonal cycle calculated from the available data, an approximation that has negligible impact on the soil moisture trends calculated for the period 2011–2020. We refer to the four time series taken from available observations and reanalysis collectively as 'environmental forcings'. The model also requires specification of four parameters at each place in space. Interested readers will find details on model development, parameter specification and the environmental forcings in Model description in Methods. By design, our historical simulation captures soil moisture trends that are driven only by variations in the environmental forcings applied to the model as we assumed that land-surface parameters remained constant throughout the historical simulation. We did not include any plant physiological processes, such as stomatal closure in response to high vapour pressure deficit (VPD)[35] and increased leaf area driven by CO_2 fertilization[36,37], in our historical simulations. We demonstrate, however, that the inclusion of plausible representations of stomatal closure and increased leaf area would make only minor contributions to the EMBM representation of historical soil moisture trends in Sensitivity analyses in Methods.

As for the available observations, the EMBM historical simulation also shows increasing summertime surface soil moisture trends across a large fraction of the continental USA (62% of the domain in the historical simulation compared with 57% in the CCI observations; Fig. 1a,c). The trends in the historical simulation explain roughly half of the spatial variance in the CCI observations taken over the same period ($r = 0.68$, $P < 0.01$). The trends in the EMBM historical simulation are also significantly ($P < 0.01$) correlated with those found in the co-located ground probes (Fig. 1d). The summertime mean surface soil moisture and the standard deviation in JJA soil moisture from the EMBM historical simulation are both significantly ($P < 0.01$) correlated with both quantities in the CCI observations and the ISMN probes across the continental USA over the period 2011–2020 (Supplementary Figs. 3 and 4).

To quantify the individual contributions of the four environmental forcings (precipitation, solar radiation, vapour pressure and snowmelt) to the trends in the EMBM historical simulation, we ran four additional experiments across the continental USA. In each experiment, three of the environmental forcings were set to their climatological seasonal cycle for all 40 years of the simulation, while the remaining forcing was identical to the one applied in the historical simulation. In the

https://doi.org/10.1038/s44221-024-00193-x

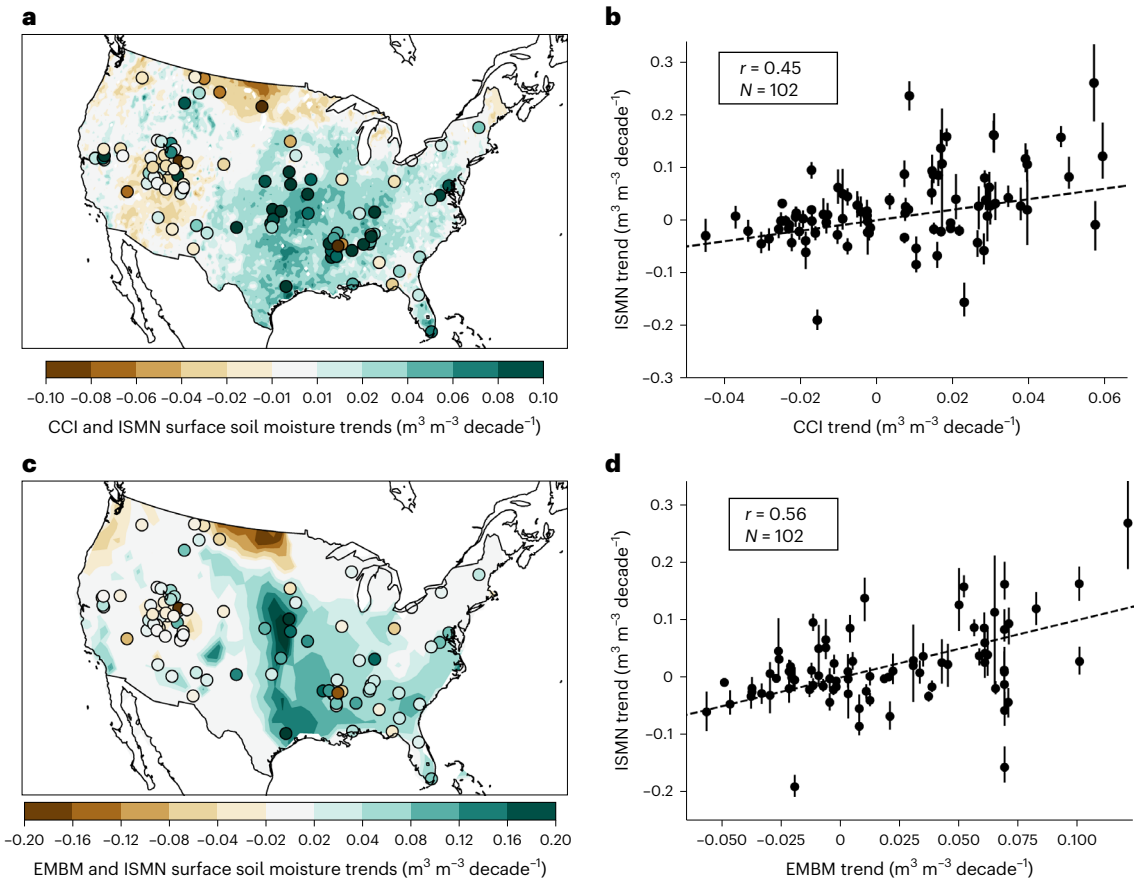

Fig. 1 | Observed and modelled soil moisture trends for the period 2011–2020. JJA surface soil moisture trends from 2011 to 2020 from observations and the EMBM. **a**,**c**, Map showing the trends from the CCI observations (**a**) and EMBM (**c**) (colour shading) and the mean estimates from 1,000 bootstrap samples of the ISMN trends (circles). Note the different colour bars in **a** and **c**. **b**,**d**, Trends from the ISMN probes as a function of the co-located trends in the CCI observations (**b**) and EMBM (**d**). The dots show the mean values from the samples and the error bars show the interquartile range of the ISMN trends from 1,000 bootstrap samples at each station. The dashed black line represents the one-to-one line, or an ideal situation where observations agree perfectly with one another, and the EMBM output. The *r* value refers to the correlation between the mean trend across the bootstrap samples from the ISMN data and the trend in the co-located CCI and EMBM data, and *N* indicates the number of points in the scatter.

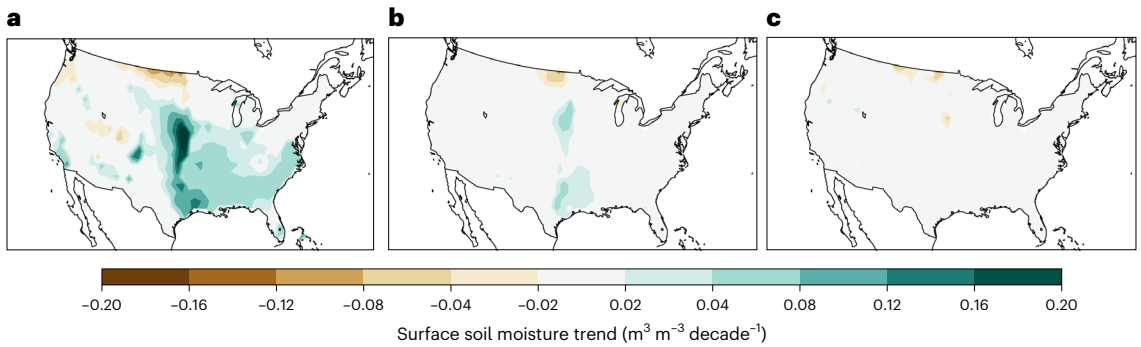

Fig. 2 | Contributions of three forcings to soil moisture trends. a–**c**, Surface soil moisture trends from the EMBM in experiments in which variations in only precipitation (**a**), solar radiation (**b**) or snowmelt (**c**) were allowed to influence the simulation. All trends were calculated for the period 2011–2020.

experiment in which only the variability in precipitation was included, the soil moisture trends from the historical simulation were largely reproduced in both their spatial pattern and magnitude (compare Figs. 2a and 1c). Variations in only solar radiation or snowmelt make smaller contributions to the soil moisture trends across the continental USA (Fig. 2b,c), and the contribution from vapour pressure is one order of magnitude smaller than these two forcings (Supplementary Fig. 5). Based on these experiments, we conclude that the observed surface soil moisture trends over the period 2011–2020 are mainly attributable to precipitation variability. This precipitation variability that drives 10-year trends in surface soil moisture is probably associated with internal variations rather than the forced response to climate change[38,39], but, as we discuss below, anthropogenic influences are expected to have a larger effect on soil moisture at longer timescales.

https://doi.org/10.1038/s44221-024-00193-x

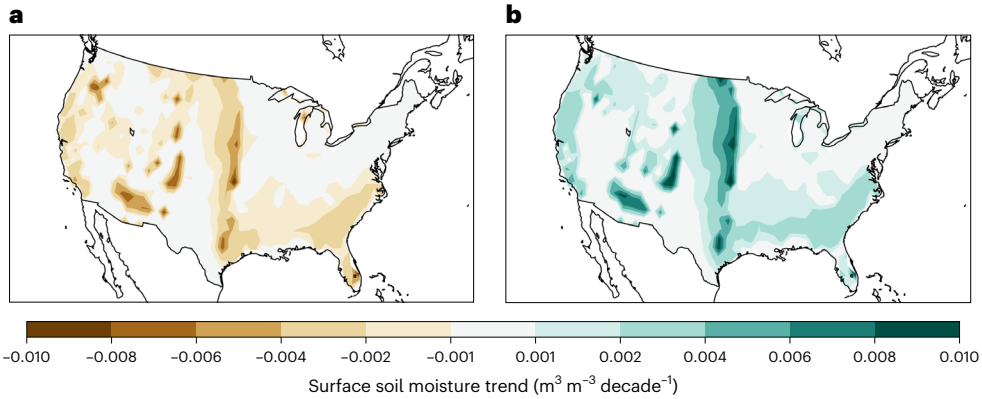

Fig. 3 | Soil moisture trends induced by warming and stomatal closure. a,**b**, JJA surface soil moisture trends derived from experiments in which the EMBM was forced by increasing only the background vapour pressure and dew point temperature (**a**) or only the vegetation resistance to transpiration in a manner that emulates stomatal closure in response to increasing atmospheric CO_2 concentrations (**b**). Results from the final 10 years of the simulations are shown.

The soil moisture tug of war

Two drivers of long-term soil moisture trends have been discussed in the literature on dryland expansion in response to anthropogenic climate change[25,27]. The first is enhanced atmospheric water vapour demand driven by higher temperatures that leads to soil drying via increased evapotranspiration[7,8]. The second is stomatal closure driven by CO_2 emissions that leads to increasing soil moisture via reduced evapotranspiration[40]. Experiments with global climate models have indicated that the plant response to CO_2 has a larger impact on column-integrated soil moisture than increased temperatures in most cases[26], although biases in climate model representations of surface soil moisture make the physical processes that drive these trends in different models unclear.

We performed two experiments using the EMBM to test how atmospheric water vapour demand and stomatal closure influence surface soil moisture and, by extension, the expansion or intensification of global drylands. In both experiments, we set the time series of precipitation, solar radiation, vapour pressure and snowmelt to their respective climatological seasonal cycles at each location to remove interannual variability in the environmental forcings. In the first experiment, we simulated the effects of global warming by adding trends to the vapour pressure and implied dew point temperature based on projected warming rates over the next four decades from a realistic CO_2 emissions scenario (Shared Socioeconomic Pathway 3–7.0 (SSP3–7.0)[41]). In the second experiment, we simulated the plant physiological response to increasing CO_2 emissions by increasing the vegetation resistance to transpiration at each location at rates determined by a recent climate model analysis[42] and the same SSP3–7.0 emissions scenario, but did not include the effects of global warming from the first experiment. For more information on the trends in vapour pressure, dew point temperature and vegetation resistance, see Warming and vegetation resistance forcings in Methods.

The soil moisture trends obtained from these atmospheric water vapour demand and stomatal closure experiments are much smaller than those observed in the historical simulation, which we identified as being largely driven by interannual precipitation variability. Widespread surface drying is present in the global warming experiment (Fig. 3a), and the magnitude of the trends is consistent with the results from general circulation model experiments[7,8]. In the plant response experiment, we found increasing soil moisture trends in regions where transpiration plays a large role in the surface energy balance (Fig. 3b).

Across the land surface, a 'tug of war' over the sign of soil moisture trends driven by anthropogenic CO_2 emissions is evident between increasing temperature leading to drying and increasing vegetation resistance to transpiration leading to reduced transpiration and moistening of the surface soil layer. These results represent a variation in the canonical 'wet get wetter, dry get drier' hypothesis for changes in the hydrological cycle driven by global warming (although the mechanism is obviously different[14,43]). We found that in regions with ample vegetation, changes in prescribed vegetation resistance to transpiration increase surface soil moisture at least as much as global warming reduces it via increased evaporative demand. In some places, the surface soil moisture trend induced by the simulated stomatal closure is larger in magnitude than the soil moisture trend induced in the experiment in which the model is forced by increasing only temperatures.

Precipitation and long-term soil moisture trends

We have already shown that the observed decadal surface soil moisture trends in the continental USA are largely attributable to interannual precipitation variability (Fig. 2). Precipitation is known to vary on timescales longer than one decade[44], and recent work has shown that random sampling of the internal variability within a large ensemble of climate model simulations can generate substantial centennial precipitation trends even without historical greenhouse gas forcing[39]. The potential for trends in precipitation at various timescales to influence soil moisture has not figured in analyses of how soil moisture will respond to climate change. In this context, we used the EMBM forced by the precipitation output from the global climate models that participated in the CMIP6 to quantify the relative influence of precipitation variability, warming and stomatal closure on surface soil moisture trends.

To quantify the contributions of these three drivers to potential soil moisture trends, we conducted four ensemble experiments over the continental USA using the EMBM. In each ensemble, we ran 23 simulations for 86 years each (2015–2100) using the precipitation output from a different CMIP6 model forced by the SSP3–7.0 emissions scenario for each simulation. For a list of the models, see CMIP6 precipitation forcing in Methods. All other environmental forcings were set to their climatological seasonal cycles. In all of the ensembles, we prescribed warming temperatures over the 86 years of each simulation using the same methodology as we used to conduct the warming simulation described above (see the discussion of Fig. 3a and Warming and vegetation resistance forcings in Methods).

In the first ensemble (Warming + Mean stomata closure + CMIP6 precipitation (P_{CMIP6}) in Fig. 4), we applied the same trend in vegetation conductance across each of the simulations as was applied in the stomatal closure experiments described above (see the discussion of Fig. 3b). This ensemble represents the 'best estimate' of future soil moisture trends given the uncertainty associated with regional temperature change, the uncertainty in plant response to increasing CO_2 and the possibility of long-term precipitation trends in response to

https://doi.org/10.1038/s44221-024-00193-x

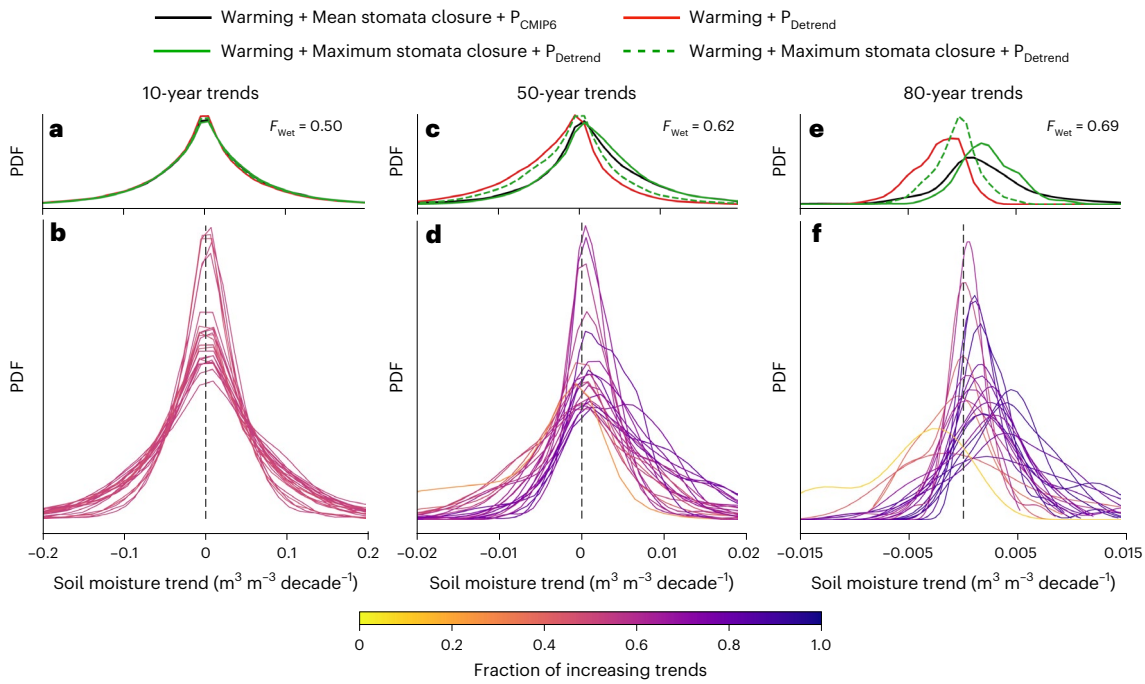

Fig. 4 | Influence of precipitation on future soil moisture trends. **a**,**c**,**e**, Probability distribution functions of 10-year (**a**), 50-year (**c**) and 80-year (**e**) surface soil moisture trends calculated across US grasslands in four ensemble experiments with the EMBM. F_{Wet} represents the average fraction of increasing soil moisture trends across space in the simulation in which CMIP6 precipitation was used as the model forcing (Warming + Mean stomata closure + P_{CMIP6}). **b**,**d**,**f**, Separate trend distributions over 10 years (**b**), 50 years (**d**) and 80 years (**f**) for each realization of the EMBM using separate CMIP6 climate model outputs as the precipitation forcing. The colours of the PDFs indicate the average spatial fraction of increasing soil moisture trends across US grasslands in the simulations; values close to zero or one indicate a high degree of spatial coherence in the soil moisture trends within each model realization.

climate change. In the remaining three ensembles, we detrended the precipitation output from CMIP6 to isolate the 'natural' precipitation variability from the potential long-term trends present in each of the CMIP6 model runs. In the second ensemble (Warming + $P_{Detrend}$ in Fig. 4), the detrended precipitation ($P_{Detrend}$) and the warming trend were the only forcings, with vegetation conductance kept constant in all simulations. The third and fourth ensembles (Warming + Maximum or Minimum stomata closure + $P_{Detrend}$ in Fig. 4) had the same precipitation and warming forcings as the second ensemble, but included trends in vegetation conductance with the magnitudes dictated by the maximum and minimum values of stomatal conductance sensitivity to CO_2 documented by Yang et al.[42].

Given the combination of (1) internal variability in precipitation, (2) uncertainty with respect to the stomatal closure effect induced by increasing CO_2 concentrations and (3) uncertainty with respect to long-term precipitation projections, what is the likelihood that changes in surface soil moisture driven by global climate change will be detectable in the coming decades? To answer this question, we computed all available 10-, 50- and 80-year soil moisture trends at each grid cell that we simulated in our ensembles after removing the first 5 years from consideration so that the EMBM has time to equilibrate. We collected the trends across all grid cells defined as 'grassland' biomes by Higgins et al.[45], which, in the USA, are centres of agriculture where soil moisture projections are extremely important for climate change impacts[3,16].

The probability distribution functions (PDFs) of the 10-year trends are nearly identical in all four of the experimental ensembles and show that increasing and decreasing soil moisture trends are roughly equally likely (Fig. 4a). These trends have magnitudes similar to those found in the ground probes and CCI observations during the period 2011–2020 and are due to the same mechanism, the internal variability in precipitation, as we have already shown that decadal soil moisture trends induced by warming and stomatal closure are an order of magnitude smaller than those driven by internal precipitation variability (compare Figs. 2 and 3).

In the first ensemble, in which the precipitation time series output from 23 CMIP6 models were used as model forcings, the 10-year trends calculated over all possible subsets in each 86-year simulation are essentially evenly divided spatially across each model (Fig. 4b). Moreover, any 10-year soil moisture trend is a poor predictor of another 10-year trend at the same place in space calculated more than 2 years later ($r < 0.2$ in all simulations), consistent with limited year-to-year memory in precipitation[39]. The presence of long-term (86-year) precipitation trends does not alter the PDFs of 10-year trends as the results from the ensemble that includes long-term precipitation trends are consistent with those from experiments in which long-term precipitation trends are removed. Thus, 10-year soil moisture trends across US grasslands should primarily be interpreted as a reflection of randomly sampled internal variability in precipitation. Similar results were obtained for US deserts and forests (Supplementary Figs. 6 and 7).

On 50-year timescales, some separation between the four ensembles is manifest across US grasslands. In the ensemble that includes only the detrended CMIP6 precipitation and increasing temperatures as model forcings (Warming + $P_{Detrend}$ in Fig. 4), 75% of all soil moisture trends are negative on 50-year timescales (Fig. 4c). If long-term trends in vegetation resistance and precipitation are included, however, the distribution tilts the other way with 62% increasing 50-year soil moisture trends. This distribution of trends is consistent across simulations as the majority of US grasslands are found to have positive trends when using precipitation output from each of the 23 CMIP6 simulations (Fig. 4d).

The results are more distinct for the 80-year trends in soil moisture. The ensemble that includes only warming and detrended precipitation variability exhibits almost entirely negative soil moisture trends (Fig. 4e). Applying the smallest documented value for stomatal

https://doi.org/10.1038/s44221-024-00193-x

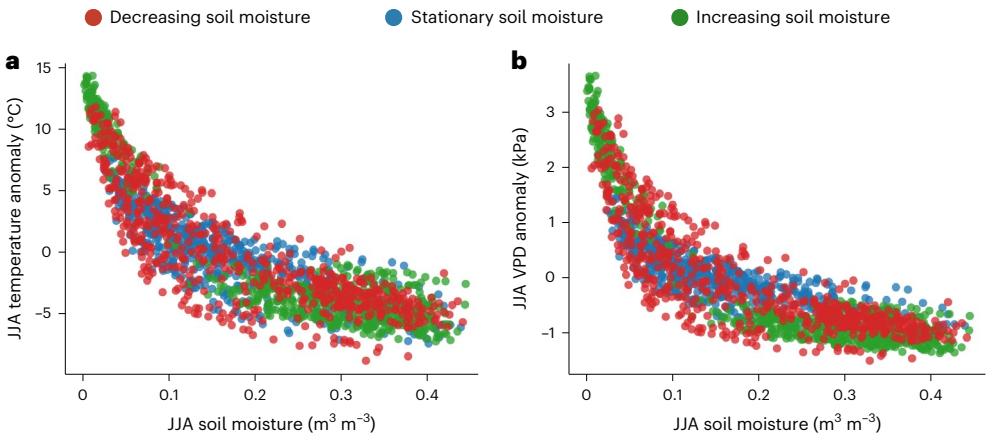

Fig. 5 | Coupling between temperature, VPD and soil moisture trends. **a**,**b**, Summertime average temperature (**a**) and VPD (**b**) as a function of summertime average surface soil moisture from our 'best estimate' ensemble (Warming + Mean stomata closure + P_{CMIP6} in Fig. 4) in simulations with decreasing soil moisture trends, nearly constant soil moisture and increasing soil moisture trends over the long term.

sensitivity to CO_2 results in an almost equal likelihood of increasing and decreasing soil moisture trends across US grasslands (Fig. 4e). If the largest stomatal sensitivity value is included, increasing soil moisture is more likely than long-term drying, with only a 35% likelihood of drying across the ensemble. In the ensemble that used CMIP6 precipitation output as an environmental forcing, increasing soil moisture trends were found across 69% of US grasslands. Unlike the 10-year trends, the 80-year trends produced by the EMBM exhibit a high degree of spatial coherence associated with the distinct trends in precipitation produced by different climate models (Fig. 4f).

Analysis of the CMIP6 models that we used in our ensemble experiments revealed that the magnitude of spread in precipitation projections over grasslands in the continental USA is common across the global land surface (Supplementary Fig. 8). However, even this spread may not truly capture the uncertainty as it represents the results from only 23 models, which is smaller than the number of simulations typically used in 'large ensemble' experiments designed to capture internal precipitation variability[46]. Although we have shown results only for grasslands, we expect our results to be general for any portion of the land surface given the inherent uncertainty in long-term precipitation projections and the possibility for random sampling of internal variability to generate trends even at centennial timescales[39]. The internal variations in precipitation at various timescales combined with the uncertainty in the forced response to climate change make it difficult to make accurate long-term soil moisture projections or indeed predict the sign of the overall trend. In addition to the analysis based on precipitation output from global climate models over US grasslands, we examined how the the same climate model precipitation output affects soil moisture trends at different timescales over US deserts and forests. In the case of deserts, where stomatal regulation plays no role in the simulations and cumulative precipitation is low, long-term trends are mostly negative (Supplementary Fig. 6). In the case of forests, the results are largely similar to those of the grasslands at all timescales, but the larger mean value of soil moisture puts a cap on the increasing soil moisture trends such that increasing and decreasing soil moisture trends become roughly equally likely (Supplementary Fig. 7). Across all biomes, the internal variations that create structural uncertainty in long-term precipitation trends are the largest contributor to uncertainty in soil moisture trends.

Conclusions

The EMBM demonstrates that interannual precipitation variability is primarily responsible for the observed decadal trends in surface soil moisture across the continental USA. On longer timescales, the best estimates of how increasing CO_2 will affect plant resistance to transpiration[40,42] suggest that increasing surface soil moisture trends driven by more efficient water use by plants will largely compensate for, and in some cases overcome, decreasing surface soil moisture trends driven by anthropogenic warming. We cannot determine the size of this effect precisely because plant responses to increasing CO_2 are imperfectly understood. Uncertainty in how plants will respond to increasing CO_2 emissions is an important contribution to the overall uncertainty in long-term trends in surface soil moisture. In particular, we did not include stomatal closure in response to high VPD or leaf area responses to increased CO_2 concentrations in our simple model, both of which may influence long-term soil moisture trends[35–37,47]. We also did not include the effects of irrigation, although these would probably offset the drying induced by warming in regions where irrigation will act as an increasingly important term in the local water budget[48].

A larger source of uncertainty in predicting future soil moisture than the plant response to increasing CO_2 concentrations comes from the fact that precipitation is highly variable on decadal and longer timescales. Our results highlight that the most important way to reduce uncertainty in soil moisture projections is to better constrain how continental precipitation will respond to climate change. The dynamic and thermodynamic responses of continental precipitation to climate change are still poorly understood[49,50], leading to uncertainty in the sign of long-term precipitation trends across a substantial fraction of Earth's land surface (Supplementary Fig. 8). Without better constraints on these projections, it is difficult to make accurate assessments of how surface soil moisture will respond to climate change.

Importantly, the presence of long-term soil moisture trends does not change the underlying relationship between temperature, VPD and soil moisture that is largely responsible for how these variables co-vary on interannual timescales. Temperature, VPD and soil moisture co-vary strongly in our model (Fig. 5) according to the non-linear relationships that have been discussed elsewhere and are driven by feedbacks that limit evaporative cooling in low VPD and high soil moisture environments[51]. It has been argued in numerous studies that warming and atmospheric drying have driven detectable changes in soil moisture at the land surface[25,52,53], but our results indicate that the co-variability in soil moisture and temperature driven by precipitation is probably responsible for any detectable soil moisture trend on timescales of less than several decades. Furthermore, our results indicate that this co-variability is likely to be independent of any underlying trend in surface soil moisture on decadal or centennial timescales.

While dryland expansion and reductions in surface soil moisture may be the null hypothesis in a warming world because the effect of

increased atmospheric demand for water vapour is fairly well constrained compared with the uncertainty in the stomatal response to CO_2 and the long-term precipitation trends, our results suggest that reduced surface soil moisture is far from a foregone conclusion across the land surface given the uncertainty in precipitation trends at each place in space. When forced with warming temperatures, the most likely value of stomatal sensitivity to CO_2 and CMIP6 precipitation output, the EMBM indicates a 69% chance of increasing soil moisture over the next 80 years in US grasslands. These trends show spatial coherence, with precipitation simulated by 5 models producing majority drying trends and 18 producing majority wetting trends. In the language of the Intergovernmental Panel on Climate Change (IPCC), this suggests that soil drying in response to climate change is 'unlikely'. However, this result is tied to a 23-member climate model ensemble that may not accurately reflect the uncertainty in long-term precipitation trends. The likelihood of increasing soil moisture, despite the tendency for soils to dry due to global warming, reflects the importance of the stomatal response to CO_2 emissions and the current uncertainties associated with precipitation variability and its potential long-term response to climate change.

Methods

Observational analysis

We used summertime (JJA) soil moisture data from the European Space Agency Climate Change Initiative (version 7) and ISMN. To extract high-quality data from probes in the ISMN, we screened out all data without a 'good' flag and then screened out summers (JJA of one year) where fewer than 45 days (out of a total of 92) of soil moisture observations were available. Only stations where more than eight summers between 2011 and 2020 met these criteria were used in our analysis. In total, 102 stations had records from 2011 to 2020 that passed this quality control procedure (see the circles in Fig. 1a).

All of the trends were calculated using an unweighted linear least-squares fit. To quantify the uncertainty in the trend estimates, we generated 1,000 bootstrap samples for each point observation (with replacement). Our central trend estimates are robust to methodology in the sense that the trend estimates calculated using unweighted least squares and those estimated using the non-parametric Thiel–Sen method gave nearly identical ISMN trends (the correlation between trends calculated by these two different methods is $r = 0.96$, Supplementary Fig. 9). We note, however, that the Thiel–Sen method generally indicates wider confidence intervals and that any analysis seeking to establish the statistical significance of observed trends may be sensitive to such methodological choices.

Model description

Equations. The governing equation for land surface temperature T is the surface energy balance:

$$\Gamma \frac{\mathrm{d}T}{\mathrm{d}t} = \mathcal{F} - F_{\mathrm{LW}} - H - L(E_{\mathrm{s}} + T_{\mathrm{s}} + T_{\mathrm{d}}), \quad (1)$$

where Γ is the heat capacity of the land surface, t is time, $\mathcal{F}$ is the net solar radiation, F_{LW} is the net longwave radiation emitted by the land surface, H is the surface sensible heat flux, E_{s}, T_{s} and T_{r} are the surface evaporation, surface transpiration and deep-layer transpiration fluxes, respectively, L is the latent enthalpy of vaporization and we have assumed that the ground heat flux is zero. All of the energy fluxes in equation (1) are measured in units of watts per square metre. The effective heat capacity Γ is a function of soil moisture:

$$\Gamma = h_{\mathrm{s}}(c_{\mathrm{s}}\rho_{\mathrm{s}} + c_{\mathrm{l}}m_{\mathrm{s}}\rho_{\mathrm{l}}), \quad (2)$$

where h_{s} is the surface layer depth, ρ_{s} and c_{s} are the density and specific heat of dry soil, respectively, and ρ_{l} and c_{l} are the density and specific heat of water, respectively. The surface layer depth was set to a constant $h_{\mathrm{s}} = 10$ cm everywhere (all spatially invariant parameter values are shown in Supplementary Table 1).

Two moisture balance equations govern volumetric soil moisture in the surface and deep layers (denoted m_{s} and m_{d}, respectively):

$$\mu_{\mathrm{s}} \frac{\mathrm{d}m_{\mathrm{s}}}{\mathrm{d}t} = \mathcal{P} + \mathcal{M} - E_{\mathrm{s}} - T_{\mathrm{s}} + C - D_{\mathrm{s}}, \quad (3)$$

$$\mu_{\mathrm{d}} \frac{\mathrm{d}m_{\mathrm{d}}}{\mathrm{d}t} = D_{\mathrm{s}} - T_{\mathrm{r}} - C - D_{\mathrm{d}}. \quad (4)$$

All of the moisture fluxes in equations (3) and (4) are given in units of kg of H_2O per m^2 per s. The parameters μ_{s} and μ_{d} describe the geometric capacity of the surface and deep layer to hold liquid water, respectively, $\mathcal{P}$ and $\mathcal{M}$ are the precipitation and snowmelt rates, respectively, C is the upward flux of soil moisture from the deep layer to the surface layer, and D_{s} and D_{d} are the downward fluxes of moisture from the surface layer to the deep layer and from the deep layer out of the model, respectively.

The soil moisture carrying capacities for the surface and deep layers μ_{s} and μ_{d} are defined as:

$$\mu_{\mathrm{s}} = h_{\mathrm{s}}\rho_{\mathrm{l}}, \quad (5)$$

$$\mu_{\mathrm{d}} = h_{\mathrm{d}}\rho_{\mathrm{l}}, \quad (6)$$

where h_{d} is the depth of the deep soil layer and was set to 90 cm. Our approach leaves out the contribution of roots deeper than 1 m to the total transpiration; we assumed that this fraction would be small on average across the continental scale that we were trying to simulate.

The net longwave radiation F_{LW} emitted by the land surface is a function of the surface and dew point temperature:

$$F_{\mathrm{LW}} = \sigma(T^4 - \epsilon\mathcal{T}_{\mathrm{D}}^4), \quad (7)$$

where σ is the Stefan–Boltzmann constant, ε is the atmospheric emissivity and $\mathcal{T}_{\mathrm{D}}$ is the time-varying dew point computed from vapour pressure forcing $\mathcal{E}(t)$. The atmospheric emissivity is given by an empirical function of $\mathcal{E}$ and ranges from 0.65 to 0.85 (ref. 54; Supplementary Table 1). The fundamental assumption underlying equation (7) is that the dew point gives an estimate of the atmosphere's temperature above the lifting condensation level that is independent of the underlying land surface and the boundary layer to which it is radiatively coupled[55]. Put a different way, we assumed that variations in the dew point temperature are more closely controlled by the ocean and atmosphere than the local land surface on monthly timescales.

The sensible heat flux is given by:

$$H = \frac{c_{\mathrm{a}}\rho_{\mathrm{a}}}{r_{\mathrm{a}}}(T - \mathcal{T}_{\mathrm{D}}), \quad (8)$$

where c_{a} and ρ_{a} are the specific heat and density of dry air, respectively, and r_{a} is the aerodynamic resistance.

Surface evaporation is given as:

$$E_{\mathrm{s}} = \frac{\rho_{\mathrm{a}}\beta_{\mathrm{s}}}{r_{\mathrm{s}}}[q_{\mathrm{s}}(T, \overline{P}) - \mathcal{Q}], \quad (9)$$

where r_{s} is the surface resistance associated with bare soil evaporation. The β_{s} factor is equal to the ratio of m_{s} and the spatially invariant field capacity θ (Supplementary Table 1) and is bounded between 0 and 1. This is a standard parameterization for soil moisture's influence on evapotranspiration that has been used in general circulation models since their initial development[56]. The saturation specific humidity q_{s} is an exponential function of surface temperature T and the local

climatological surface pressure $\bar{P}$. The same surface pressure was used to calculate the specific humidity forcing $\mathcal{Q}$ from vapour pressure observations $\mathcal{E}$. We ignored temporal fluctuations in surface pressure and used annual mean values from ERA5 for $\bar{P}$ at each place in space that we simulated. Surface evaporation was set to zero in the rare cases that the near surface humidity difference $q_s - \mathcal{Q}$ is less than zero. As our primary interest was summertime, when surface air is rarely saturated, we did not include condensation in our consideration of the energy and moisture budgets.

Similar to surface evaporation, we can write the surface and deep-layer transpiration terms as:

$$T_s = \frac{\rho_a \mathcal{R} \beta_s}{r_v}[q_s(T, \bar{P}) - \mathcal{Q}], \tag{10}$$

$$T_d = \frac{\rho_a (1 - \mathcal{R}) \beta_d}{r_v}[q_s(T, \bar{P}) - \mathcal{Q}], \tag{11}$$

where r_v is the vegetation resistance to transpiration and $\mathcal{R}$ is the fraction of total roots that derive their moisture from the surface layer. The parameter β_d is analogous to β_s in equation (9), except that the deep-layer soil moisture value was used to compute the degree to which deep-layer transpiration is limited by available soil moisture.

The drainage fluxes D_s and D_d are given by:

$$D_s = \frac{\mu_s (m_s - m_d) \mathcal{H}(m_s - m_d)}{\mathrm{d}t}, \tag{12}$$

$$D_d = \frac{\mu_d (m_d - \theta) \mathcal{H}(m_d - \theta)}{\mathrm{d}t}, \tag{13}$$

where $\mathcal{H}$ is the Heaviside function and dt is the timescale of model integration. The assumption underlying equation (12) is that the surface layer cannot be more saturated than the deep layer because the gravitational force is so much stronger than any possible driver of upward soil moisture flux. If precipitation or snowmelt leads to a situation where $m_s > m_d$, equation (12) indicates that the excess moisture is immediately injected into the deep soil layer. Equation (13) indicates that if the deep layer exceeds the field capacity, the excess moisture is purged from the model as drainage (or run-off).

The soil moisture layers interact through the upward soil moisture flux C:

$$C = \rho_l \upsilon_C (m_d - m_s) \mathcal{H}(m_d - m_s), \tag{14}$$

where υ_C is the speed at which the two soil moisture layers equilibrate in the absence of evapotranspiration or precipitation. This parameterization of the upward soil moisture flux can incorporate both capillary action and hydraulic redistribution by plant roots, which are known to contribute a large water flux in many deep-rooted ecosystems[57]. In contrast to the drainage fluxes, we assumed that the upward soil moisture flux acts only when the surface layer is less saturated than the deep layers.

Model integration. For all simulations, we initialized the model on 1 January with completely saturated soil and a surface temperature of 280 K. The results are insensitive to changes in these initial values. The surface fluxes were calculated at each time step according to the parameterizations described above, and the Euler method was used to integrate the equations forward in time. Ten time steps per day were used to integrate the equations forward, although our model is stable for time steps as short as three steps per day.

Parameters. In addition to the environmental forcings, the model requires the specification of five parameters (r_s, r_v, r_a, $\mathcal{R}$ and υ_C) at each place in space. To guide our choices, we used the biomes defined by Higgins et al. (hereafter H16)[45], who divided the land surface into categories based on vegetation height (either 'tall' or 'short') and ecosystem productivity ('high', 'medium' or 'low'). For our purposes, the entirety of the continental USA is divided into deserts, grasslands and forests. For deserts, only r_s, υ_C and r_a were specified because we assumed that transpiration was zero. In grasslands ('short' vegetation with 'medium' or 'high' productivity in the language of H16) and forests ('tall' vegetation in the language of H16), the deep root fraction was determined from the grassland and temperate forest values reported by Jackson et al.[58]. The values of aerodynamic resistance r_a for these three ecosystems are proportional to the values of Raupach[59], but an order of magnitude larger because we used the dew point rather than the air temperature at 2 m as a forcing in the EMBM (equation (8)). We used the three case studies detailed below to understand the sensitivity of the model to the parameters r_v, r_s and υ_C and selected values that characterize the three biomes to extrapolate across the entire continental USA. All of the parameter choices that vary across space are shown in Supplementary Table 2.

Case study 1

In our first case study, we examined soil moisture data from Porter Canyon (39.28° N, 117.37° W) in the Nevada Desert, a site operated by the US Geological Survey as part of the Snow Telemetry Network. As noted above, we set the root fraction $\mathcal{R}$ to zero and prescribed an infinite vegetation resistance r_v to eliminate transpiration in this desert biome defined by H16. The two other parameters to be specified were the bare soil evaporative resistance r_s and the upward soil moisture flux velocity υ_C. Supplementary Fig. 10a,b shows how the mean and interannual variability of JJA surface soil moisture are impacted by changes in the parameters r_s and υ_C. Unsurprisingly, we found that lower evaporative resistance values lead to drier soils (via increased evaporation) and higher upward soil moisture flux velocities lead to wetter soils (via more efficient recharge of the surface soil by the deep layer). The connection between mean soil moisture and interannual variability is more nuanced. For low r_s values, the high evaporative demand in the desert leads to completely dry soils every summer, which reduces the variability in m_s. For extremely high r_s values, decreased evaporation leads to saturated soils every summer and also reduces the interannual variability. The highest values of $\sigma(m_s)$ overlap with intermediate values of mean JJA soil moisture, a result that characterizes our other case studies (see below).

Supplementary Fig. 10a,b shows that many (r_s, υ_C) pairs reproduce both the mean and variability in JJA surface soil moisture found in the ISMN measurements at Porter Canyon. However, the parameter choices also impact the seasonal cycle of surface and deep soil moisture, temperature and latent heat flux, as shown in Supplementary Fig. 10c–f. The darkest black line shows the simulation in which the surface layer is effectively decoupled from the surface (by using a very low value of υ_C); this simulation has an exaggerated seasonal cycle of surface soil moisture relative to the cycle measured by the ground probes of the ISMN and the deep soil moisture is nearly constant and unrealistically high (off the scale shown in Supplementary Fig. 10d). The lightest grey line shows the simulation in which the surface and deep layers are tightly coupled (υ_C is high). In this simulation, the seasonal cycle in surface moisture is damped relative to the cycle revealed by ISMN probes in this location and the mean soil moisture at depth is lower than observed. This suggests that the surface and deep layers are coupled too closely in this simulation. We set the (r_s, υ_C) pair for desert environments based on the middle simulation (intermediate grey line in Supplementary Fig. 10c–f). The seasonal cycle of latent heat flux in ERA5 is most closely captured by the first simulation in which the surface and deep layers are decoupled, but as the main objective of this study was to understand variations in m_s, we selected $r_s = 125$ s m^{-1} and $\upsilon_C = 5 \times 10^{-7}$ m s^{-1} as the values of these parameters that represent all 'desert' biomes in our

regional simulations. We define a desert as a region with both 'short' vegetation and 'low' productivity as defined by H16.

Case study 2

In the second case study, we examined a grassland site in Minnehaha County, South Dakota (43.7° N, 96.6° W) operated by the Soil Climate Analysis Network. We used root fraction $\mathcal{R}$ and surface resistance r_a values from the literature cited above, and set r_s to 1,000 s m^{-1} to reduce bare soil evaporation in these environments, where we assumed that transpiration was the dominant surface water flux (aside from precipitation). Similar to the case study above, we performed sensitivity tests to investigate how the EMBM representation of the mean state surface soil moisture and summertime variability depends on the vegetation resistance r_v and the coupling velocity of the two soil moisture layers υ_C. The mean state surface soil moisture was found to be insensitive to the coupling velocity υ_C (Supplementary Fig. 11a). In contrast to the mean state, the variability in summertime surface moisture decreases as the two layers become more tightly coupled (Supplementary Fig. 11b). We found that uncoupling the two soil layers (by decreasing υ_C) allows for extreme drying during some summers that is not found in the ISMN observations and leads to increased year-to-year variability. Across the $r_v = 50$ s m^{-1} contour, where the mean state surface soil moisture produced by the EMBM matches the observations, the EMBM variability is higher than observed. As this bias is reduced at higher values of the coupling velocity and the seasonal cycles of all relevant state variables and fluxes are insensitive to changing this parameter (Supplementary Fig. 11c–f), we chose $r_v = 50$ s m^{-1} and $\upsilon_C = 1 \times 10^{-5}$ m s^{-1} to represent grasslands (Supplementary Table 2). Grasslands are defined as regions with 'short' vegetation that have either 'medium' or 'high' productivity in H16.

Case study 3

No soil moisture probes in the ISMN that are situated in forests met our quality control procedure outlined above. To understand how the EMBM simulates soil moisture in forested environments, we took surface soil moisture data from Blodgett Forest (38.90° N, 120.63° W) in California, operated by the AmeriFlux network. Again, we set r_s to a low value (1,000 s m^{-1}) to suppress surface evaporation. Supplementary Fig. 12a,b shows the sensitivity of summertime soil moisture statistics to changes in the parameters r_v and υ_C. The most important distinction between the forested site and the other two case studies is the sensitivity of the model output to changes in the coupling velocity. High values of υ_C are required to match the summertime mean surface soil moisture found in the ISMN and CCI observations. Unlike the South Dakota site, the climate in California is dry during the summer and tighter coupling between the two soil layers is required to sustain meaningful surface moisture through months with low average rainfall (Supplementary Fig. 12a). While the model underestimates the observed interannual variation in summertime surface moisture from the AmeriFlux network (off the scale in Supplementary Fig. 12b), the EMBM variability is maximized for higher υ_C values. However, Supplementary Fig. 12c–f shows that a very high coupling velocity leads to a more exaggerated seasonal cycle than the $\upsilon_C = 1 \times 10^{-7}$ m s^{-1} and $r_v = 300$ s m^{-1} values that we chose to represent forests. Forests are defined as any region that has 'tall' vegetation in H16, but based on the ERA5 latent heat flux output, we made a final modification and decreased r_v to 100 s m^{-1} for 'high' productivity forests defined in H16 that encompass much of the southeastern USA where no forest ISMN or AmeriFlux probes are available (Supplementary Table 2).

Sensitivity analyses

Number of model layers. The model described above is based entirely on two model layers, but a variety of models with different numbers of layers and layer thicknesses have been proposed to represent soil moisture dynamics at various timescales[60]. To understand the sensitivity of the EMBM to the number of model layers, we conducted a set of sensitivity experiments in three different case study regions (the Nevada Desert, grasslands in South Dakota and a high-productivity forest in Georgia). In the first experiment, we used a 1-m-thick 'slab' of soil as the only layer in the model (which correspondingly had no upward soil moisture flux). In each of the following nine experiments, we added a 10 cm layer from the surface downward coupled together with capillary and drainage fluxes given by equations (12)–(14). The transpiration from each model layer was determined using equation (10) with the root fraction for deeper layers given by the exponentially diminishing profiles in Jackson et al.[58]. The configuration of our EMBM is one 10 cm surface layer atop a 90 cm soil slab. Removing the 10 cm surface layer generally decreases run-off and increases soil moisture, whereas adding additional deeper 10 cm layers has only a minor effect on the mean and variance (Supplementary Fig. 13).

To understand how our trend estimates are influenced by adding additional model layers, we conducted an additional historical simulation with a five-layer version of the model. The soil moisture trends from historical simulations using this five-layer model are highly correlated ($r = 0.92$, $P < 0.01$, Supplementary Fig. 14) with the soil moisture trends produced by our default, two-layer version of the model (that is, the historical EMBM simulation). We stress that this does not indicate that model layers are not important for some applications, such as resolving shorter-term soil moisture variations where a more detailed treatment of soil moisture movement may be critical (for example, see refs. 61,62).

VPD dependence of stomatal closure and CO_2-induced changes in leaf area index. To understand how the EMBM is sensitive to (1) including a humidity dependence in the equation for stomatal conductance or (2) CO_2-induced changes in leaf area index (LAI), we performed two additional simulations with the historical forcings described above over the period 1981–2020. In the first, we included an empirical model of stomatal closure:

$$g_s = g_o - \alpha \ln(\mathrm{VPD}), \tag{15}$$

where $g_o = 1/r_v$ and α was set such that $\alpha/g_o = 0.6$, a constant ratio found across ecosystems[63]. While recent work has shown that this parameterization probably overestimates the contribution of plant physiology to evapotranspiration[64], it is a standard parameterization that is similar to the Ball–Berry and Medlyn models of stomatal closure and does not require assumptions about carbon assimilation rates, which are outside the scope of this paper[65]. Using the parameterization in equation (15) (rather than keeping r_v constant over time, as we did in our historical simulation), we found that trends over the decade 2011–2020 are generally insensitive to including stomatal sensitivity to VPD (Supplementary Fig. 15a).

To understand whether CO_2-induced changes in the LAI may have influenced our estimation of historical trends, we relied on a previously published analysis to quantify the effect of changing LAI on vegetation resistance to evapotranspiration. Wang et al.[66] have shown that the LAI has increased by around 0.05–0.1 m^2 leaf area per m^2 ground area (0.05–0.1 m^2 m^{-2}) per decade from 2001 to 2017 across vegetated regions of the continental USA, where the background LAI is between 3 and 5 m^2 m^{-2} according to Verger et al.[67]. This corresponds to a 1–3% per decade increase in LAI; we assumed a linear scaling between percentage changes in LAI and decreasing vegetation resistance to transpiration. We applied this 1–3% per decade decrease in r_v to an additional historical simulation for the period 1981–2020 to investigate whether our estimation of historical soil moisture trends is sensitive to including CO_2-driven changes in LAI. We found that soil moisture trends in a simulation with CO_2-driven changes in LAI are extremely well correlated with soil moisture trends in our historical simulation in which these changes were not included ($r = 0.95$, Supplementary Fig. 15b), indicating that LAI trends have limited importance for historical soil moisture variability over the period 2011–2020.

Warming and vegetation resistance forcings

In the experiments performed to understand the soil moisture response to global warming and stomatal closure, we ran the EMBM for 40 years with the environmental forcings set to their respective climatological seasonal cycles at each location. To emulate global warming, we added a trend to the vapour pressure forcing expected from the warming of the oceans by 1.8 °C over the 40 years of the simulation while maintaining constant relative humidity. The vapour pressure forcing $\mathcal{E}_W(t)$ applied to the model in the warming simulations is given by:

$$\mathcal{E}_W(t) = \mathcal{E}_H(t) + e_s[T_D(t)] - e_s(\overline{T_D}), \quad (16)$$

where $\mathcal{E}_H(t)$ is the climatological seasonal cycle of vapour pressure, e_s is the saturation vapor pressure, and $T_D(t)$ is a linear increase of 1.8 °C over the 40-year simulation from the climatological mean dew point temperature $\overline{T_D}$ at each place in space. Supplementary Fig. 16 shows the warming rate that manifests in our warming simulations when equation (16) was applied to the model. The warming rate in the simulations is consistent with the rates from global climate models, and the spatial pattern is magnified in dry regions, which is also expected.

In the experiment designed to emulate plant response to climate change, we assumed that the stomatal sensitivity of 0.09% ppm^{-1} CO_2 found by Yang et al.[42] is correct and that CO_2 concentrations will rise by approximately 180 ppm over the next four decades, consistent with the SSP3–7.0 scenario[41]. We therefore applied a 16.2% change in vegetation resistance to transpiration over our 40-year simulation shown in Fig. 3b. For the ensembles in Fig. 4 and Supplementary Figs. 6 and 7, we used a range of CO_2 sensitivities found in the Yang et al. study and assumed a 450 ppm increase in atmospheric CO_2 concentrations over the next 100 years (also consistent with the SSP3–7.0 scenario). The mean value of stomatal sensitivity to CO_2 is 0.09% ppm^{-1}, with a minimum sensitivity of 0.05% ppm^{-1} and a maximum sensitivity of 0.15% ppm^{-1}.

CMIP6 precipitation forcing

Twenty-three climate models were used to produce Fig. 4 and Supplementary Figs. 6–8: ACCESS-CM2, AWI-CM-1-1-MR, BCC-CSM2-MR, CanESM5, CESM2-WACCM, CMCC-CM2-SR5, EC-Earth3-AerChem, EC-Earth3, EC-Earth3-Veg-LR, EC-Earth3-Veg, FGOALS-f3-L, FGOALS-g3, GFDL-ESM4, INM-CM4-8, INM-CM5-0, IPSL-CM6A-LR, KACE-1-0-G, MIROC6, MPI-ESM-1-2-HR, MPI-ESM1-2-LR, MRI-ESM2-0, NorESM2-LM and NorESM2-MM.

Reporting summary

Further information on research design is available in the Nature Portfolio Reporting Summary linked to this article.

Data availability

All of the data used in this study are publicly available.

Code availability

The python code for the EMBM is available at https://github.com/Lvargaszeppetello/Two_Layer.

References

1. Wasko, C., Nathan, R. & Peel, M. C. Changes in antecedent soil moisture modulate flood seasonality in a changing climate. *Water Resour. Res.* **56**, e2019WR026300 (2020).
2. Sazib, N., Bolten, J. D. & Mladenova, I. E. Leveraging NASA Soil Moisture Active Passive for assessing fire susceptibility and potential impacts over Australia and California. *IEEE J. Sel. Top. Appl. Earth Obs. Remote Sens.* **15**, 779–787 (2021).
3. Rigden, A., Mueller, N., Holbrook, N., Pillai, N. & Huybers, P. Combined influence of soil moisture and atmospheric evaporative demand is important for accurately predicting US maize yields. *Nat. Food* **1**, 127–133 (2020).
4. Vargas Zeppetello, L. R., Battisti, D. S. & Baker, M. B. The physics of heat waves: what causes extremely high summertime temperatures? *J. Clim.* **35**, 2231–2251 (2022).
5. McColl, K. A., He, Q., Lu, H. & Entekhabi, D. Short-term and long-term surface soil moisture memory time scales are spatially anticorrelated at global scales. *J. Hydrometeorol.* **20**, 1165–1182 (2019).
6. Stahl, M. O. & McColl, K. A. The seasonal cycle of surface soil moisture. *J. Clim.* **35**, 4997–5012 (2022).
7. Berg, A., Sheffield, J. & Milly, P. C. Divergent surface and total soil moisture projections under global warming. *Geophys. Res. Lett.* **44**, 236–244 (2017).
8. Cook, B. I. et al. Twenty-first century drought projections in the CMIP6 forcing scenarios. *Earths Future* **8**, e2019EF001461 (2020).
9. Western, A. W., Grayson, R. B. & Blöschl, G. Scaling of soil moisture: a hydrologic perspective. *Annu. Rev. Earth Planet. Sci.* **30**, 149–180 (2002).
10. Famiglietti, J. S., Ryu, D., Berg, A. A., Rodell, M. & Jackson, T. J. Field observations of soil moisture variability across scales. *Water Resour. Res.* **44**, W01423 (2008).
11. Montzka, C. et al. Validation of spaceborne and modelled surface soil moisture products with cosmic-ray neutron probes. *Remote Sens.* **9**, 103 (2017).
12. Short Gianotti, D. J. et al. Landscape water storage and subsurface correlation from satellite surface soil moisture and precipitation observations. *Water Resour. Res.* **55**, 9111–9132 (2019).
13. Feldman, A. et al. Remotely sensed soil moisture can capture dynamics relevant to plant water uptake. *Water Resour. Res.* **59**, e2022WR033814 (2022).
14. Feng, H. & Zhang, M. Global land moisture trends: drier in dry and wetter in wet over land. *Sci. Rep.* **5**, 18018 (2015).
15. Dorigo, W. et al. Evaluating global trends (1988–2010) in harmonized multi-satellite surface soil moisture. *Geophys. Res. Lett.* **39**, L18405 (2012).
16. Proctor, J., Rigden, A., Chan, D. & Huybers, P. More accurate specification of water supply shows its importance for global crop production. *Nat. Food* **3**, 753–763 (2022).
17. Yuan, S., Quiring, S. M. & Leasor, Z. T. Historical changes in surface soil moisture over the contiguous United States: an assessment of CMIP6. *Geophys. Res. Lett.* **48**, e2020GL089991 (2021).
18. Koster, R. D. et al. On the nature of soil moisture in land surface models. *J. Clim.* **22**, 4322–4335 (2009).
19. Qiao, L., Zuo, Z. & Xiao, D. Evaluation of soil moisture in CMIP6 simulations. *J. Clim.* **35**, 779–800 (2022).
20. Trugman, A., Medvigy, D., Mankin, J. & Anderegg, W. Soil moisture stress as a major driver of carbon cycle uncertainty. *Geophys. Res. Lett.* **45**, 6495–6503 (2018).
21. Lian, X. et al. Multifaceted characteristics of dryland aridity changes in a warming world. *Nat. Rev. Earth Environ.* **2**, 232–250 (2021).
22. Scheff, J. & Frierson, D. M. Terrestrial aridity and its response to greenhouse warming across CMIP5 climate models. *J. Clim.* **28**, 5583–5600 (2015).
23. Huang, J., Yu, H., Guan, X., Wang, G. & Guo, R. Accelerated dryland expansion under climate change. *Nat. Clim. Change* **6**, 166–171 (2016).
24. Dai, A., Zhao, T. & Chen, J. Climate change and drought: a precipitation and evaporation perspective. *Curr. Clim. Change Rep.* **4**, 301–312 (2018).
25. Denissen, J. et al. Widespread shift from ecosystem energy to water limitation with climate change. *Nat. Clim. Change* **12**, 677–684 (2022).
26. Swann, A. L., Hoffman, F. M., Koven, C. D. & Randerson, J. T. Plant responses to increasing CO_2 reduce estimates of climate impacts on drought severity. *Proc. Natl Acad. Sci. USA* **113**, 10019–10024 (2016).

27. Berg, A. & McColl, K. A. No projected global drylands expansion under greenhouse warming. *Nat. Clim. Change* **11**, 331–337 (2021).
28. IPCC. in *Climate Change 2021: The Physical Science Basis* (eds Masson-Delmotte, V. et al.) (Cambridge Univ. Press, 2021).
29. Al-Yaari, A. et al. Assessment and inter-comparison of recently developed/reprocessed microwave satellite soil moisture products using ISMN ground-based measurements. *Remote Sens. Environ.* **224**, 289–303 (2019).
30. Dorigo, W. et al. ESA CCI soil moisture for improved Earth system understanding: state-of-the art and future directions. *Remote Sens. Environ.* **203**, 185–215 (2017).
31. Harris, I., Osborn, T. J., Jones, P. & Lister, D. Version 4 of the CRU TS monthly high-resolution gridded multivariate climate dataset. *Sci. Data* **7** 109 (2000).
32. Loeb, N. G. et al. Clouds and the Earth's Radiant Energy System (CERES) Energy Balanced and Filled (EBAF) top-of-atmosphere (TOA) edition-4.0 data product. *J. Clim.* **31**, 895–918 (2018).
33. Hersbach, H. et al. The ERA5 global reanalysis. *Q. J. R. Meteorol. Soc.* **146**, 1999–2049 (2020).
34. Xie, Y., Gibbs, H. K. & Lark, T. J. Landsat-based Irrigation Dataset (LANID): 30 m resolution maps of irrigation distribution, frequency, and change for the US, 1997–2017. *Earth Syst. Sci. Data* **13**, 5689–5710 (2021).
35. Grossiord, C. et al. Plant responses to rising vapor pressure deficit. *New Phytol.* **226**, 1550–1566 (2020).
36. Kovenock, M., Koven, C. D., Knox, R. G., Fisher, R. A. & Swann, A. L. Leaf trait plasticity alters competitive ability and functioning of simulated tropical trees in response to elevated carbon dioxide. *Global Biogeochem. Cycles* **35**, e2020GB006807 (2021).
37. Zhang, Y. et al. Increasing sensitivity of dryland vegetation greenness to precipitation due to rising atmospheric CO_2. *Nat. Commun.* **13**, 4875 (2022).
38. Rasmusson, E. M. & Arkin, P. A. A global view of large-scale precipitation variability. *J. Clim.* **6**, 1495–1522 (1993).
39. McKinnon, K. A. & Deser, C. The inherent uncertainty of precipitation variability, trends, and extremes due to internal variability, with implications for western US water resources. *J. Clim.* **34**, 9605–9622 (2021).
40. Ainsworth, E. A. & Rogers, A. The response of photosynthesis and stomatal conductance to rising CO_2: mechanisms and environmental interactions. *Plant Cell Environ.* **30**, 258–270 (2007).
41. Meinshausen, M. et al. The shared socio-economic pathway (SSP) greenhouse gas concentrations and their extensions to 2500. *Geosci. Model Dev.* **13**, 3571–3605 (2020).
42. Yang, Y., Roderick, M. L., Zhang, S., McVicar, T. R. & Donohue, R. J. Hydrologic implications of vegetation response to elevated CO_2 in climate projections. *Nat. Clim. Change* **9**, 44–48 (2019).
43. Held, I. M. & Soden, B. J. Robust responses of the hydrological cycle to global warming. *J. Clim.* **19**, 5686–5699 (2006).
44. Tsonis, A. Widespread increases in low-frequency variability of precipitation over the past century. *Nature* **382**, 700–702 (1996).
45. Higgins, S. I., Buitenwerf, R. & Moncrieff, G. R. Defining functional biomes and monitoring their change globally. *Global Change Biol.* **22**, 3583–3593 (2016).
46. Deser, C. et al. Isolating the evolving contributions of anthropogenic aerosols and greenhouse gases: a new CESM1 large ensemble community resource. *J. Clim.* **33**, 7835–7858 (2020).
47. Yuan, W. et al. Increased atmospheric vapor pressure deficit reduces global vegetation growth. *Sci. Adv.* **5**, 1396 (2019).
48. Chen, X. et al. Detecting significant decreasing trends of land surface soil moisture in eastern China during the past three decades (1979–2010). *J. Geophys. Res. Atmos.* **121**, 5177–5192 (2016).
49. Emori, S. & Brown, S. Dynamic and thermodynamic changes in mean and extreme precipitation under changed climate. *Geophys. Res. Lett.* **32**, L17706 (2005).
50. Shiogama, H., Watanabe, M., Kim, H. & Hirota, N. Emergent constraints on future precipitation changes. *Nature* **602**, 612–616 (2022).
51. Vargas Zeppetello, L. R., Battisti, D. S. & Baker, M. B. The origin of soil moisture evaporation 'regimes'. *J. Clim.* **32**, 6939–6960 (2019).
52. Abatzoglou, J. T. & Williams, A. P. Impact of anthropogenic climate change on wildfire across western US forests. *Proc. Natl Acad. Sci. USA* **113**, 11770–11775 (2016).
53. Ellis, T. M., Bowman, D. M., Jain, P., Flannigan, M. D. & Williamson, G. J. Global increase in wildfire risk due to climate-driven declines in fuel moisture. *Global Change Biol.* **28**, 1544–1559 (2022).
54. Staley, D. & Jurica, G. Effective atmospheric emissivity under clear skies. *J. Appl. Meteorol. Climatol.* **11**, 349–356 (1972).
55. Vargas Zeppetello, L. R., Donohoe, A. & Battisti, D. Does surface temperature respond to or determine downwelling longwave radiation? *Geophys. Res. Lett.* **46**, 2781–2789 (2019).
56. Manabe, S. Climate and the ocean circulation: I. The atmospheric circulation and the hydrology of the Earth's surface. *Mon. Weather Rev.* **97**, 739–774 (1969).
57. Neumann, R. B. & Cardon, Z. G. The magnitude of hydraulic redistribution by plant roots: a review and synthesis of empirical and modeling studies. *New Phytol.* **194**, 337–352 (2012).
58. Jackson, R. B. et al. A global analysis of root distributions for terrestrial biomes. *Oecologia* **108**, 389–411 (1996).
59. Raupach, M. Vegetation–atmosphere interaction and surface conductance at leaf, canopy and regional scales. *Agric. For. Meteorol.* **73**, 151–179 (1995).
60. Guswa, A. J., Celia, M. A. & Rodriguez-Iturbe, I. Models of soil moisture dynamics in ecohydrology: a comparative study. *Water Resour. Res.* **38**, 1166 (2002).
61. Vrettas, M. D. & Fung, I. Y. Sensitivity of transpiration to subsurface properties: exploration with a 1-D model. *J. Adv. Model. Earth Syst.* **9**, 1030–1045 (2017).
62. Cueto-Felgueroso, L., Suarez-Navarro, M. J., Fu, X. & Juanes, R. Interplay between fingering instabilities and initial soil moisture in solute transport through the vadose zone. *Water* **12**, 917 (2020).
63. Oren, R. et al. Survey and synthesis of intra- and interspecific variation in stomatal sensitivity to vapour pressure deficit. *Plant Cell Environ.* **22**, 1515–1526 (1999).
64. Vargas Zeppetello, L. R. et al. Apparent surface conductance sensitivity to vapour pressure deficit in the absence of plants. *Nat. Water* **1**, 941–951 (2023).
65. Novick, K. A. et al. The increasing importance of atmospheric demand for ecosystem water and carbon fluxes. *Nat. Clim. Change* **6**, 1023–1027 (2016).
66. Wang, M., Chen, J. M. & Wang, S. Reconstructing the seasonality and trend in global leaf area index during 2001–2017 for prognostic modeling. *J. Geophys. Res. Biogeosci.* **125**, 2020–005698 (2020).
67. Verger, A., Baret, F., Weiss, M., Filella, I. & Peñuelas, J. Geoclim: a global climatology of LAI, FAPAR, and FCOVER from VEGETATION observations for 1999–2010. *Remote Sens. Environ.* **166**, 126–137 (2015).

Acknowledgements

L.R.V.Z. thanks the James S. McDonnell Foundation and the Harvard University Center for the Environment. A.M.T. thanks CONACyT, Fundación México en Harvard, and the Instituto de Inovación y Transferencia de Tecnología. P.H. thanks the Sahara Project.

Author contributions

L.R.V.Z. designed the EMBM, performed the analysis and wrote the first draft of the paper, and all authors contributed to the revisions. A.M.T. provided quality control validation for the soil moisture datasets and proposed measures to ensure statistical robustness. P.H. proposed the project, helped to write the paper and gave important suggestions to the section of the paper that concerns uncertainty in precipitation projections under climate change.

Competing interests

The authors declare no competing interests.

Additional information

Supplementary information The online version contains supplementary material available at https://doi.org/10.1038/s44221-024-00193-x.

Correspondence and requests for materials should be addressed to Lucas R. Vargas Zeppetello.

Peer review information *Nature Water* thanks the anonymous reviewers for their contribution to the peer review of this work.

nature portfolio

Corresponding author(s): Lucas R. Vargas Zeppetello

Last updated by author(s): Dec 27, 2023

Reporting Summary

Nature Portfolio wishes to improve the reproducibility of the work that we publish. This form provides structure for consistency and transparency in reporting. For further information on Nature Portfolio policies, see our Editorial Policies and the Editorial Policy Checklist.

Statistics

For all statistical analyses, confirm that the following items are present in the figure legend, table legend, main text, or Methods section.

n/a	Confirmed	
☐	☒	The exact sample size (*n*) for each experimental group/condition, given as a discrete number and unit of measurement
☐	☒	A statement on whether measurements were taken from distinct samples or whether the same sample was measured repeatedly
☐	☒	The statistical test(s) used AND whether they are one- or two-sided *Only common tests should be described solely by name; describe more complex techniques in the Methods section.*
☐	☒	A description of all covariates tested
☐	☒	A description of any assumptions or corrections, such as tests of normality and adjustment for multiple comparisons
☐	☒	A full description of the statistical parameters including central tendency (e.g. means) or other basic estimates (e.g. regression coefficient) AND variation (e.g. standard deviation) or associated estimates of uncertainty (e.g. confidence intervals)
☒	☐	For null hypothesis testing, the test statistic (e.g. *F*, *t*, *r*) with confidence intervals, effect sizes, degrees of freedom and *P* value noted *Give P values as exact values whenever suitable.*
☒	☐	For Bayesian analysis, information on the choice of priors and Markov chain Monte Carlo settings
☒	☐	For hierarchical and complex designs, identification of the appropriate level for tests and full reporting of outcomes
☒	☐	Estimates of effect sizes (e.g. Cohen's *d*, Pearson's *r*), indicating how they were calculated

Our web collection on statistics for biologists contains articles on many of the points above.

Software and code

Policy information about availability of computer code

Data collection	All data are from publicly available data sets
Data analysis	Custom code is written in python and is available at the link described in our code availability statement.

For manuscripts utilizing custom algorithms or software that are central to the research but not yet described in published literature, software must be made available to editors and reviewers. We strongly encourage code deposition in a community repository (e.g. GitHub). See the Nature Portfolio guidelines for submitting code & software for further information.

Data

Policy information about availability of data

All manuscripts must include a data availability statement. This statement should provide the following information, where applicable:

- Accession codes, unique identifiers, or web links for publicly available datasets
- A description of any restrictions on data availability
- For clinical datasets or third party data, please ensure that the statement adheres to our policy

All data used in this study is publicly available.

Research involving human participants, their data, or biological material

Policy information about studies with human participants or human data. See also policy information about sex, gender (identity/presentation), and sexual orientation and race, ethnicity and racism.

Reporting on sex and gender	N/A
Reporting on race, ethnicity, or other socially relevant groupings	N/A
Population characteristics	N/A
Recruitment	N/A
Ethics oversight	N/A

Note that full information on the approval of the study protocol must also be provided in the manuscript.

Field-specific reporting

Please select the one below that is the best fit for your research. If you are not sure, read the appropriate sections before making your selection.

☐ Life sciences ☐ Behavioural & social sciences ☒ Ecological, evolutionary & environmental sciences

For a reference copy of the document with all sections, see nature.com/documents/nr-reporting-summary-flat.pdf

Ecological, evolutionary & environmental sciences study design

All studies must disclose on these points even when the disclosure is negative.

Study description	Understanding observed soil moisture trends over the past ten years, and the soil moisture response to climate change
Research sample	Observed soil moisture taken from in-situ measurements and satellite-derived product.
Sampling strategy	All good quality data were used. To determine robustness of trend estimates, we used a 10,000 sample bootstrap method with replacement.
Data collection	No data collection was done associated with this study.
Timing and spatial scale	Seasonal data across the continental united states
Data exclusions	All quality control flags were removed from the analysis.
Reproducibility	All model experiments are described in detail in the text
Randomization	No allocation/randomization was performed
Blinding	N/A

Did the study involve field work? ☐ Yes ☒ No

Reporting for specific materials, systems and methods

We require information from authors about some types of materials, experimental systems and methods used in many studies. Here, indicate whether each material, system or method listed is relevant to your study. If you are not sure if a list item applies to your research, read the appropriate section before selecting a response.

Materials & experimental systems

n/a	Involved in the study
☒	☐ Antibodies
☒	☐ Eukaryotic cell lines
☒	☐ Palaeontology and archaeology
☒	☐ Animals and other organisms
☒	☐ Clinical data
☒	☐ Dual use research of concern
☒	☐ Plants

Methods

n/a	Involved in the study
☒	☐ ChIP-seq
☒	☐ Flow cytometry
☒	☐ MRI-based neuroimaging

Plants

Seed stocks	N/A
Novel plant genotypes	N/A
Authentication	N/A